Fission of heavy hypernuclei formed in antiproton annihilation

T. A. Armstrong,[1] J. P. Bocquet,[2] G. Ericsson,[3] T. Johansson,[3]
T. Krogulski,[4],* R. A. Lewis,[1] F. Malek,[2],† M. Maurel,[5] E. Monnand,[5]
J. Mougey,[6] H. Nifenecker,[2] J. Passaneau,[1] P. Perrin,[5] S. M. Polikanov,[7]
M. Rey-Campagnolle,[8],‡ C. Ristori,[5] G. A. Smith,[1] and G. Tibell[3]

[1] *Pennsylvania State University, University Park, Pennsylvania 16802*
[2] *Institut des Sciences Nucléaires, Institut National de Physique Nucléaire et de Physique des Particles, Centre National de la Recherche Scientifique and University of Grenoble, CEDEX, France*
[3] *Department of Radiation Sciences, Uppsala University, P.O. Box 535, S-75121 Uppsala, Sweden*
[4] *Warsaw University, Bialystok Branch, PL-15-424 Bialystok, Poland*
[5] *DRFMC, Centre d'Etudes Nucléaires de Grenoble, Boîte Postale 85X, 38041 Grenoble, France*
[6] *Continuous Electron Beam Accelerator Facility, Newport News, Virginia 23606*
[7] *Gesellschaft für Schwerionenforschumg Darmstadt, Postfach 110541, D-6100 Darmstadt, Germany*
[8] *Centre de Spectrométrie Nucléaire et de Spectrométrie de Masse, Institut National de Physique Nucléaire et de Physique des Particles, Centre National de la Recherche Scientifique, F-91405 Orsay, France*

(Received 5 August 1992)

Heavy hypernuclei are produced in the annihilation of antiprotons in ^{238}U. The delayed fission of heavy hypernuclei and hypernuclei of fission fragments are observed by using the recoil-distance method in combination with measurement of secondary electron multiplicity. The lifetime of hypernuclei in the region of uranium is found to be $(1.25 \pm 0.15) \times 10^{-10}$ sec. It is observed that Λ hyperons predominantly stick to the heavier fission fragments. The yield of hypernuclei is found to be $(7.4 \pm 1.7) \times 10^{-3}$ per stopped antiproton. No coincidences with K^+ were found. Statistical and systematic errors on the number of events expected do not rule out this possibility.

PACS number(s): 21.80.+a, 25.85.−w, 27.90.+b

I. INTRODUCTION

In previous papers we reported results of a search for heavy hypernuclei produced in the annihilation of antiprotons in ^{238}U [1] and ^{209}Bi [2]. The underlying idea of the experiment was that the nonmesonic decay of the Λ hyperon in a heavy hypernucleus leads to an excitation of the residual nucleus to an energy sufficient to induce fission. Thus, the decay of heavy hypernuclei would be observed as delayed fission with the lifetime of the hypernucleus.

The Λ hyperon can be produced in a secondary interaction of K mesons after $\bar{p}N$ annihilation with residual nuclei. More exotic reactions, such as the direct production of Λ hyperons on pairs of nucleons, are also possible [3].

The annihilation of antiprotons in nuclei is accompanied by the emission of mesons and nucleons, giving the residual nucleus a rather high recoil momentum. This makes it possible to employ, in the study of heavy hypernuclei, the recoil-distance technique, earlier used in studies of short-lived fission isomers [4]. The characteristic feature of this technique is the experimental geometry which provides a strong suppression of prompt fission fragments, with a detection efficiency for delayed fission of about 1%.

The delayed fission lifetimes observed in the annihilation of antiprotons in ^{238}U and ^{209}Bi were found to be $0.1^{+0.1}_{-0.05}$ nsec [1] and $0.25^{+0.25}_{-0.10}$ nsec [2], respectively. It was assumed that the lifetimes measured are related to groups of nuclides in the vicinity of U and Bi, respectively.

As seen from the accuracy of the quoted results, it was impossible to conclude whether the probability of nonmesonic decay for these two groups of nuclei is the same or not. The shorter lifetime in the case of uranium may result from the fact that the recoil-distance technique, although providing separation of delayed and prompt fission, does not exclude completely the recording of hypernuclei of fission fragments which are produced in the prompt fission of excited hypernuclei. Because of the high fissility of nuclei in the uranium region, the number of detected hypernuclei of fission fragments can be rather large. As will be discussed below this may result in too short a lifetime for delayed fission for the ^{238}U target.

Here we report results obtained with an improved experimental apparatus. It allowed us to impose additional criteria for the separation of prompt-fission events and thus made it possible to separate the delayed fission, caused by the decay of the Λ hyperon, from the hyper-

*Present address: Gesellschaft für Schwerionenforschumg Darmstadt, Postfach 110541, D-6100 Darmstadt, Germany.
†Present address: Institut de Physique, Institut National de Physique Nucléaire et de Physique des Particles, Centre National de la Recherche Scientifique and the University of Lyon, Lyon, France.
‡Present address: CERN/PPE, CH-1211 Gènève, Switzerland.

nuclei of fission fragments. This was achieved by using the fact that fission fragments cause the emission of a large number of secondary electrons when they leave the target surface [5]. In contrast, when a slow heavy recoil is knocked out of the target, the number of secondary electrons is small.

The data on hypernuclei of fission fragments can be used in the analysis of the prompt fission of excited hypernuclei. We can understand the appearance of hypernuclei of fission fragments by using rather simple assumptions concerning the nonmesonic decay of a Λ hyperon. The possibility of explaining two different types of events using the same assumption on the nonmesonic decay of hypernuclei would be an additional argument in favor of the hypernuclear nature of the observed effect.

Furthermore, a detector was implemented to record K^+ mesons in coincidence with fission fragments. The observation of kaons in coincidence with events identified as the prompt or delayed fission of hypernuclei would be a direct confirmation of this identification.

In Sec. I the experimental setup is described. In Sec. II the experimental results are presented. In Sec. III we present the results of the data analysis performed on the assumption that the effect observed is related to the decay of hypernuclei, and in Sec. IV the results obtained are discussed.

II. EXPERIMENTAL SETUP

A. Principle and general description

Figure 1(a) shows schematically how delayed-fission fragments are recorded by the recoil-distance method. In the case of prompt fission which occurs inside the target, the fission fragments cannot hit that part of the detector which is shadowed by the target backing (the hatched part). The delayed fission occurs in vacuum, at a certain distance from the target plane. This distance is determined by the velocity and lifetime of the recoiling nucleus. In this case the fragments can hit the shadowed area of the detector. Thus, the signature of delayed fission would be that a fission fragment is recorded in this part of the detector.

In principle, the scheme shown in Fig. 1(a) provides reliable suppression of the prompt-fission fragments at a level of at least 10^{-6}. However, the situation turns out to be somewhat different when it is used in the study of hypernuclei. There, in addition to hypernuclei of heavy elements, there are also hypernuclei of fission fragments produced as the result of the prompt fission of excited hypernuclei. Since the hypernuclei of fission fragments are emitted from the target, they cannot hit the shadowed area of the detector. However this is true only if we ignore the decay of the Λ hyperon in a moving fragment.

Because of the relatively high velocity of fission fragments (about 10^{10} mm/sec) the mean distance the fragments travel before the Λ hyperon decays is about 2 mm, comparable to the size of the target. Since in the region of the fission-fragment masses the nonmesonic decay predominates, we may expect that in this decay the fission fragment receives a momentum which cannot be

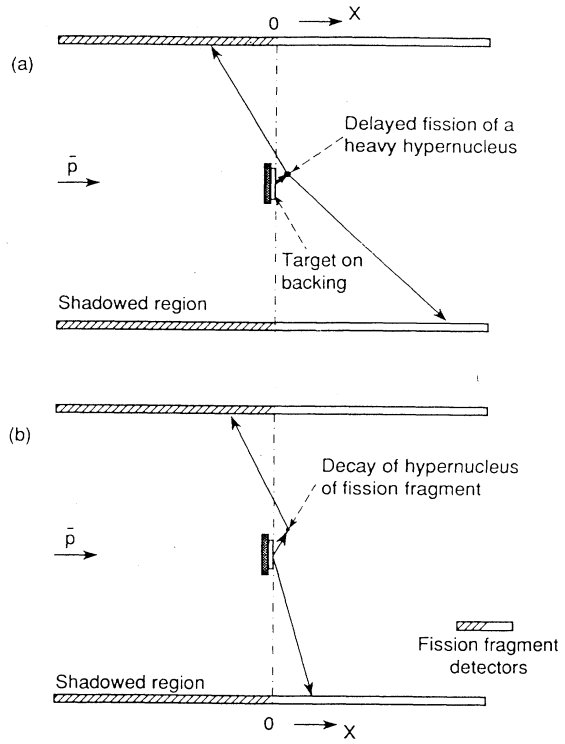

FIG. 1. Schematic representation of the recoil-distance method as applied to the study of (a) delayed fission of heavy hypernuclei, and (b) decay of hypernuclei of fission fragments. Both types of events can provide hits in the shadowed region (hatched) of the detectors while prompt fission cannot.

neglected. In a nonmesonic decay on a free nucleon the nucleons produced would have momenta of 400 MeV/c. When this decay occurs inside the nucleus, the Fermi motion of nucleons, as well as the rescattering of the nucleons produced, should be taken into account. It is then plausible to expect that the distribution of the momentum transfer to the fragments is broad and extends to several hundreds of MeV/c. Consequently, although the momentum transfer from the Λ decay is appreciably lower than the momentum of a fission fragment (about 4000 MeV/c), it is still sufficiently high to deflect the initial trajectory of the fragment. As a result, some fragments could hit the shadowed area of the detector near the target plane [Fig. 1(b)].

To distinguish between the delayed fission of heavy hypernuclei and the decay of hypernuclei of fission fragments, we made use of the following fact: While the delayed fission of heavy hypernuclei occurs in vacuum, the hypernuclei of prompt-fission fragments are emitted from the target. In the latter case some tens of slow secondary electrons are emitted as a result of the interaction of the fragments with the surface layer of the target. A slow recoiling nucleus leaves the target with appreciably lower velocity than fission fragments and will thus produce fewer secondary electrons. Therefore, by measuring the number of low energy secondary electrons one can distinguish between these types of events. This was done

using an electron detector placed in front of the target and operating in coincidence with the fission-fragment detectors. Those fragments which were recorded in the shadowed area of the detectors and accompanied by the emission of a large number of electrons were attributed to the hypernuclei of fission fragments, and the rest of the shadow events attributed to delayed fission. The threshold of the electron detector could be set to such a low level that practically all delayed fission events were accompanied by a small but measurable signal from the detector.

In Fig. 2 we show the scheme of the whole experimental setup. The antiproton beam passed successively through the 0.1 mm Be window of the beam tube, a 3×7 mm^2 slit in a scintillator used as an active collimator, and through a variable Mylar degrader. It was further slowed down in the plastic scintillator which served both as target backing and beam detector. Some antiprotons were stopped in the U target deposited on this scintillator, where they were captured to form antiprotonic atoms of uranium. The subsequent annihilation of antiprotons can induce many different processes. Some of these may lead to the formation of hypernuclei of residual excited nuclei which either undergo prompt or—after the emission of neutrons and mesons— delayed fission. In both cases the fission fragments are detected in coincidence by a pair of parallel plate avalanche counters (PPAC's) placed perpendicularly to the target plane at a distance of 270 mm. The electron detector was positioned in front of the target at a distance of about 5 mm. The front face of the kaon detector was at 45 cm from the target, behind one of the PPAC's subtending 16% of the full solid angle.

B. Fission-fragment detectors

The two PPAC's, 190×290 mm^2 each, consisted of two planes of horizontal and vertical wires placed between two outer cathode planes and one central anode plane.

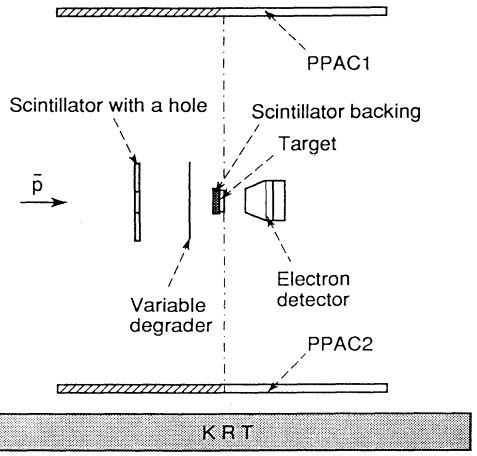

FIG. 2. Scheme of the experimental setup (not to scale). PPAC is the parallel plate avalanche counter; KRT is the Kaon range telescope.

They were filled with isobutane at a pressure of 7 Torr, and separated from the volume of the reaction chamber by 2 μm thick Mylar foils. The position resolution of the chambers along the beam direction and in the perpendicular direction was found to be 1.0 and 1.8 mm, respectively. In addition, recording independently fast anode pulses, we obtained a timing signal needed for time-of-flight (TOF) measurements and the amplitude of anode pulses and thus the specific ionization of the detected particles. Combining these data for each event, it was possible to discriminate fission fragments from any background due to light particles from $\bar{p}$ annihilation.

C. Target arrangement

The ^{238}U target was deposited, by ion implantation, on a 0.2 mm thick plastic scintillator backing, as a spot 2×5 mm^2 of 0.2 mg/cm^2 thickness. The target surface was flat within 1 μm. Backings with two different widths, 2.5 and 8.0 mm, were used. The scintillator provided the zero-time signal required in the TOF measurement. An additional adjustable degrader, placed before the scintillator, optimized the stopping rate of antiprotons in the uranium target.

D. Secondary-electron detector

A microchannel plate electron multiplier (MCP) was used to detect secondary electrons produced in the interaction of fission fragments and recoil nuclei with the target. The pulse height of the signal from the MCP detector is proportional to the number of secondary electrons. The mean value of this number for fission fragments is approximately 180, and an order of magnitude lower for recoiling hypernuclei. The electrons were accelerated and focused by an electric field of 5 kV between the target and the entrance of the MCP detector. Microchannel detectors demand a vacuum of 10^{-7} Torr to perform in a stable way. The leakage of isobutane through the windows of the fission counters did not permit such a vacuum in the whole volume of the reaction chamber. It could be sustained locally around the target and MCP by an additional cryogenic pump. Nevertheless, in the course of the experiment, the MCP detector had to be replaced to ensure a proper response.

E. K^+ meson detector

In the present experiment a kaon range telescope (KRT) was also used. A detailed description of the KRT is given in Ref. [6]. It is a rectangular parallelepiped $100 \times 100 \times 50$ cm^3, composed of 100 cells constructed with alternating plates of copper and acrylic scintillator. It provides coarse tracking in three dimensions as well as energy loss and timing information. Both the scintillator and the copper serve as moderators, contributing roughly equally to the energy loss. The stopped K^+ mesons decay in the KRT ($K^+ \to \mu^+ \nu$ or $\pi^+ \pi^0$) with a mean life of 12 nsec. The signals from the cells are identified in two groups, the first one corresponding to the stopped

K meson and the second one to the pion or muon from its decay. The momentum range of the detected kaons was $250 < P_k < 750$ MeV/c, the upper limit being determined by the thickness of the KRT, and the lower limit by attenuation in material between the target and the KRT.

III. EXPERIMENTAL RESULTS

The experiment was carried out at the CERN Low Energy Antiproton Ring, LEAR, using a $\bar{p}$ beam with 105 MeV/c momentum. A total of 2.5×10^{10} and 1.6×10^{10} antiprotons were delivered on the ^{238}U targets deposited on 2.5 and 8 mm wide scintillators, respectively. As a result, 1128 "shadow events" with one fragment detected in the shadowed zone of the PPAC's and the complementary fragment in the nonshadowed area were recorded in the first case and 350 in the second case. It should be noted that, compared to the previous measurements [1, 2], there was an appreciable number (139) of double-hit events, with two fission fragments detected in the shadowed area. Only about 1% of the antiprotons are stopped in the target material. With the present geometry of the experiment (Fig. 2), a significant fraction of the antiprotons are stopped in the MCP detector holder whose front end is viewed by the shadowed area of the PPAC's. The double-hit events may arise from antiproton induced prompt fission of impurities on this front end. This assumption agrees with the result of an additional experiment with a 2.5 mm wide scintillator without target material. Here, four double-hit events were registered with 2×10^9 incoming antiprotons.

A data-acquisition system based on CAMAC operating under a NORD computer control was used to record the data. A registered event consisted of the space-time coordinates of the incident hits in the PPAC's and KRT, the amplitude of the corresponding analogue pulses, as well as the amplitude and timing signals from the MCP detector. The MCP and PPAC's were calibrated with a ^{252}Cf source in 4π geometry.

Figure 3 shows the two-dimensional distributions dE/dx vs TOF obtained from the PPAC's with the U target (deposited on the 2.5 mm wide scintillator) irradiated with antiprotons. Here (a) corresponds to events with both fragments registered in the nonshadowed area of the PPAC's (prompt fission) and (b) to events with one fragment detected in the shadowed part. The results for both types of events are consistent with the calibration data from the fission fragments of ^{252}Cf. In Fig. 4 the corresponding pulse-height distributions obtained from the MCP detector are presented. Figure 5 shows the two-dimensional TOF spectrum of fission fragments for (a) prompt fission and (b) shadow events. Both cases correspond to symmetric fission. Fig. 5(a) shows that even for prompt fission, where the counting rate was relatively high, the contribution from random coincidences was negligible.

A comparison of the pulse-height distributions of signals from the MCP detector, for prompt fission [Fig. 4(a)] and for the shadow events [Fig. 4(b)], shows that for prompt fission there is one broad peak. This peak is located in the same region as the one obtained in the ^{252}Cf calibration. The shadow events, however, are divided into two groups. One of them is centered around channel 1000 and the other group is located below channel 250. We attribute the first group to prompt fission of excited hypernuclei, i.e., to those cases when one of the fragments, as a result of the Λ-hyperon decay, is deflected into the shadowed area of the PPAC. The second group is assumed to be due to fission events resulting from the decay of heavy hypernuclei. It was found in the analysis that practically all shadow events were accompanied by a signal from the MCP detector. This is taken as an indication that the electrons were detected with an efficiency

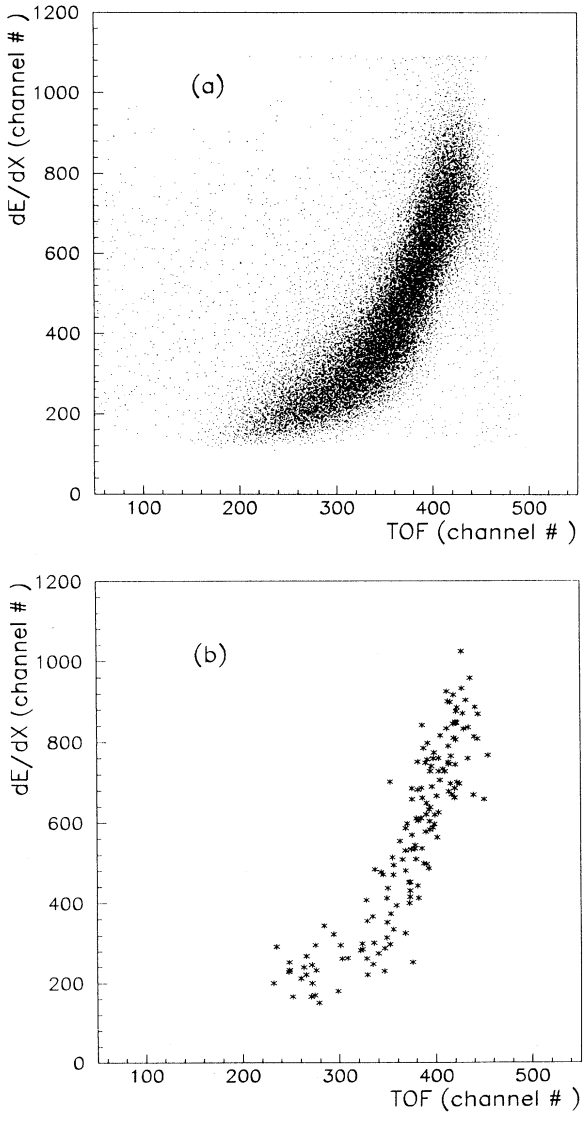

FIG. 3. dE/dx vs TOF (time of flight between target backing scintillator and PPAC) measured with the PPAC's for two types of events: (a) both fragments in coincidence are in the nonshadowed area, and (b) one of the fragments is in the shadowed area.

close to 100%.

The main conclusions drawn from the experimental distributions in Figs. 3–5 are the following: (i) there are two types of shadow events, one due to the hypernuclei of fission fragments and the other to delayed fission of heavy hypernuclei and (ii) the fission is symmetric both for prompt and delayed events.

In the following we perform an analysis of our results based on these conclusions. The experimental coordinate distributions for fission fragments are compared with those obtained in a Monte Carlo simulation to be described later. In order to simplify the discussion, we confine ourselves to the distributions in the coordinate along the axis, here denoted by X, which is directed perpendicular to the target plane with positive and negative values of X downstream and upstream of the target, respectively (Fig. 1). This is the coordinate for which the dependence of the shadow effect upon the characteristics of the nonmesonic decay (lifetime and momentum transfer) is seen in the most transparent way. In fact, the coordinate distributions along the axis parallel to the target plane should depend only weakly on the lifetime of hypernuclei and the momentum transfer in the Λ decay.

In Fig. 6 we show the experimental X coordinate distributions of shadow events accompanied by a small or large number of secondary electrons. We attribute these two distributions to the delayed fission of heavy hypernuclei and to hypernuclei of fission fragments, respectively. They are clearly different both in the shadowed and nonshadowed areas of the detector. The events corresponding to hypernuclei of fission fragments are localized closer

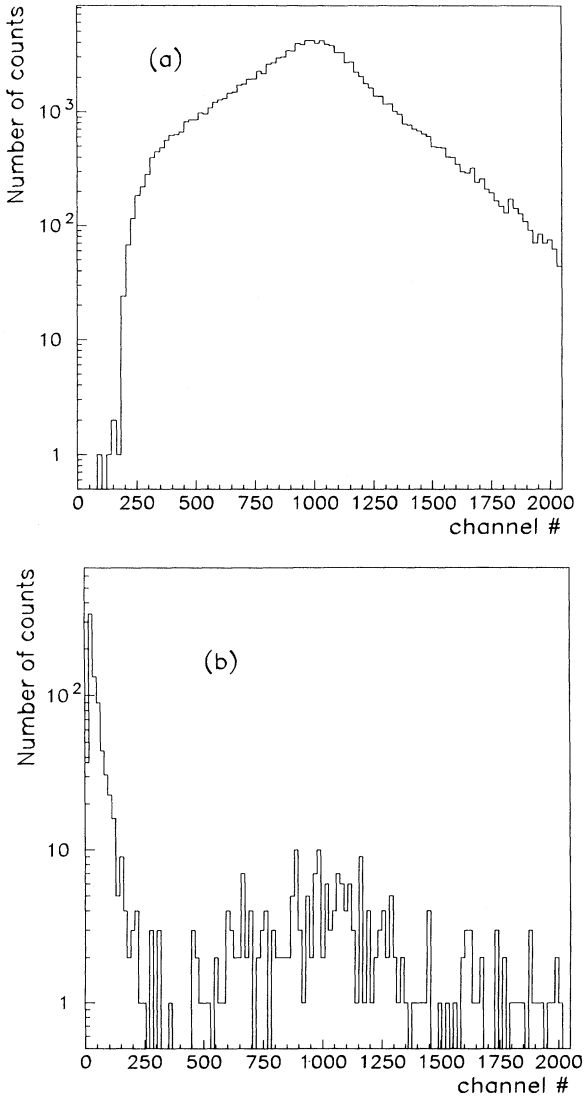

FIG. 4. Amplitude spectrum given by the MCP for events with (a) both fragments in coincidence in the nonshadowed area and (b) one of the fragments in the shadowed area.

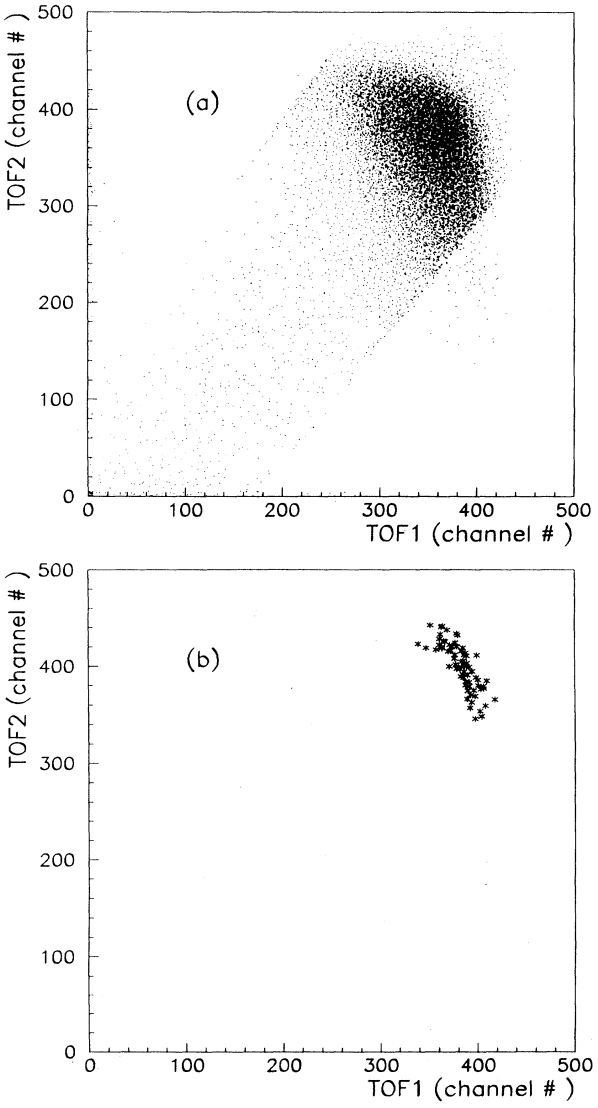

FIG. 5. Time of flight of one fragment vs time of flight of the other for events with (a) both fragments in coincidence in the nonshadowed area, and (b) one of the fragments in the shadowed area.

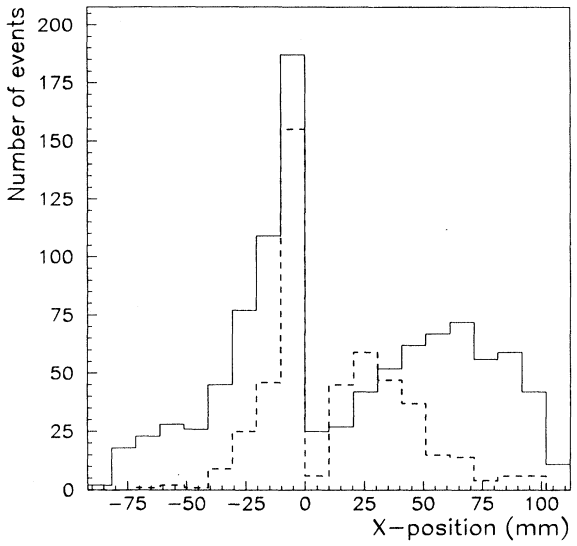

FIG. 6. X-position distributions of coincident fragments in the PPAC's for events with one fragment in the shadowed area. The solid and dashed lines represent the events accompanied by a low- and high-amplitude MCP signal, respectively.

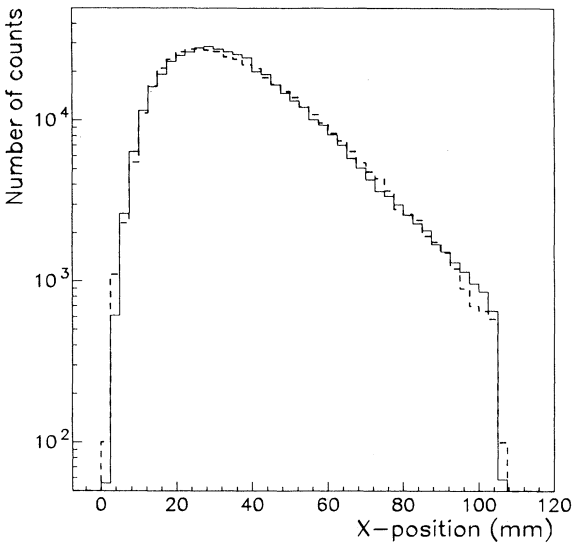

FIG. 7. X-position distributions of the prompt-fission fragments in the PPAC's (solid line); the dashed line was obtained with the Monte Carlo simulation.

to the target plane, and their coordinate distribution in the shadowed area is steeper.

During the experiment K^+ mesons were registered in coincidence with fission fragments. Thus, 436 K^+ mesons were observed in coincidence with 1.25×10^6 prompt-fission events. No coincidences were observed with the shadow events.

IV. DATA ANALYSIS

A. Prompt fission

The sample of events with two fragments detected in coincidence in the nonshadowed area of the PPAC's is mainly due to prompt fission induced by stopped antiprotons. It also contains a small admixture ($\sim 10^{-3}$) of events from prompt and delayed fission of hypernuclei which can be neglected at this stage of analysis. The prompt fission is a result of antiproton annihilation through many channels, in which the residual nucleus is excited to an energy above the fission barrier. Here, the antiproton induced fission will not be analyzed in detail; it has been studied independently [7] showing a symmetric mass distribution of fission fragments which is centered at $M = 106$ u with a dispersion $\sigma(M) = 22$ u. Only those characteristics which help to better describe the production of hypernuclei will be investigated here.

In the case of prompt fission both fragments hit the PPAC's in the nonshadowed zone. The X position distribution is in this case determined by the momentum distribution of excited nuclei produced in the annihilation, the geometry of the PPAC's, and the energy loss of the fragments in the target. In Fig. 7 the solid line shows the X-position distribution of the prompt-fission events measured in the experiment. The rather strong decrease in the distribution near the target plane reflects the absorption in the target and the PPAC windows. The slope of the distribution at large distances from the target plane is due to the decreasing contribution of high momentum recoils. These effects were taken into account by using a geometrical detection efficiency determined from the X distribution measured for single-fission fragments.

In the same phenomenological approach as used previously [1, 2], the isotropic momentum distribution of fissioning nuclei was approximated by the function

$$N(p) = p^{n/2}\exp(-p/p_0) \ , \tag{1}$$

where p_0 and n are free parameters. In fact, there is a third nonexplicit parameter involved, namely a cutoff, $p_{\max}$, for acceptable values of the momentum of the fissioning nucleus. The dashed line in Fig. 7 is the result of the simulation obtained with the parameter values of $n = 2$, $p_0 = 400$ MeV/c, $p_{\max} = 2000$ MeV/c. Using the number of fission fragments recorded, their detection efficiency in the PPAC's (see Sec. IV D), and the corresponding number of $\bar{p}$ stopped in the U target, it is possible to calculate the probability of prompt fission of ^{238}U induced by stopped antiprotons. This probability was found to be (85±15)% which agrees with the estimate of [8].

B. Hypernuclei of fission fragments

The analysis of the hypernuclei of fission fragments, i.e., of shadow events accompanied by the emission of a large number of secondary electrons, is based on the model discussed in Sec. II A.

As a first stage of the process we consider the antiproton annihilation which leads to the production of an ex-

cited hypernucleus. The momentum distribution of these hypernuclei is assumed to be isotropic and given by the expression in Eq. (1). This is a purely phenomenological approach, in which we neglect details of the various processes governing the momentum distribution of the hypernuclei.

The second step of this process is the prompt fission of the excited hypernucleus. One of the fragments produced carries the Λ hyperon which undergoes nonmesonic decay $\Lambda + N \rightarrow N + N$. The lifetime for this decay is assumed to be 2.5×10^{-10} sec, i.e., close to the free Λ lifetime .

When an excited hypernucleus undergoes fission, the Λ hyperon sticks to one of the fission fragments. The probability of the Λ sticking can be a function of the fission-fragment mass.

It is clear that the Λ particle must have been initially attached to the fragment detected in the shadowed region. The mass of this fragment relative to that of the original fissioning hypernucleus can be determined by means of the double velocity technique. This technique is based upon the fact that nucleon evaporation from the fragments after fission has forward-backward symmetry in the fragment frame, and, therefore, does not change the fragment velocity on the average. If 1 and 2 label the fission fragments, momentum conservation at the time of fission gives the following relation between masses and velocities:

$$M_1/(M_1 + M_2) = V_2/(V_1 + V_2) \ . \tag{2}$$

This relation added to the conservation of velocities on the average provides the ratio $R_1 = M_1/(M_1 + M_2)$ from the measurement of the velocities of the two fragments. Here it is sufficient to have the velocities in relative units (see also Sec. IV C). The attachment probability of the Λ particle to a fragment of mass M_1, $A_\Lambda(R_1)$, can be expressed in terms of the counting rate $N_{F\Lambda}(R_1)$ of fission fragments observed in the shadowed region in coincidence with a complementary fragment in the nonshadowed region, with a high MCP signal, and a corresponding mass ratio R_1 (see the appendix).

Figure 8(a) gives the variation of the experimental ratio $N_{F\Lambda}(R_1)/[N_{F\Lambda}(R_1) + N_{F\Lambda}(R_2)]$ (dashed line) as a function of R_1, and of the same ratio corrected for the fragment mass resolution and for the difference in detection efficiency between light and heavy fragments (solid line). The last one shows the variation of the attachment probability of the Λ particle to the fragment of mass M_1. A clear positive correlation is observed implying that high mass fragments are detected in a greater number in the shadowed region than are low mass fragments. The correlation observed in Fig. 8(a) for the corrected histogram can be described by the relation

$$A_\Lambda(R) = 0.5 + 1.7(R - 0.5) \ . \tag{3}$$

Figure 8(b) is the same as Fig. 8(a) but for delayed hypernucleus fission (low MCP amplitudes). No apparent correlation between the two ratios is found. This was expected since, in the case of the decay of heavy hypernuclei outside the target, no preference should exist for a light or a heavy fragment to be detected in the shadowed region.

While the data on the TOF (velocity) of fragments in the shadow events provide information on the Λ-hyperon attachment to fission fragments, the X distribution can be used to obtain information on the momentum transfer in the nonmesonic Λ-hyperon decay. In the analysis of this distribution we assume that the probability of the Λ-hyperon attachment is proportional to the fragment mass. The calculation of the deflection of the fragments to the shadowed area involves only the momenta of the fragments, which in binary fission are the same for heavy and light fragments. Therefore, the results of the calculation of the momentum transfer in the Λ-hyperon decay depends very little on the assumption about the

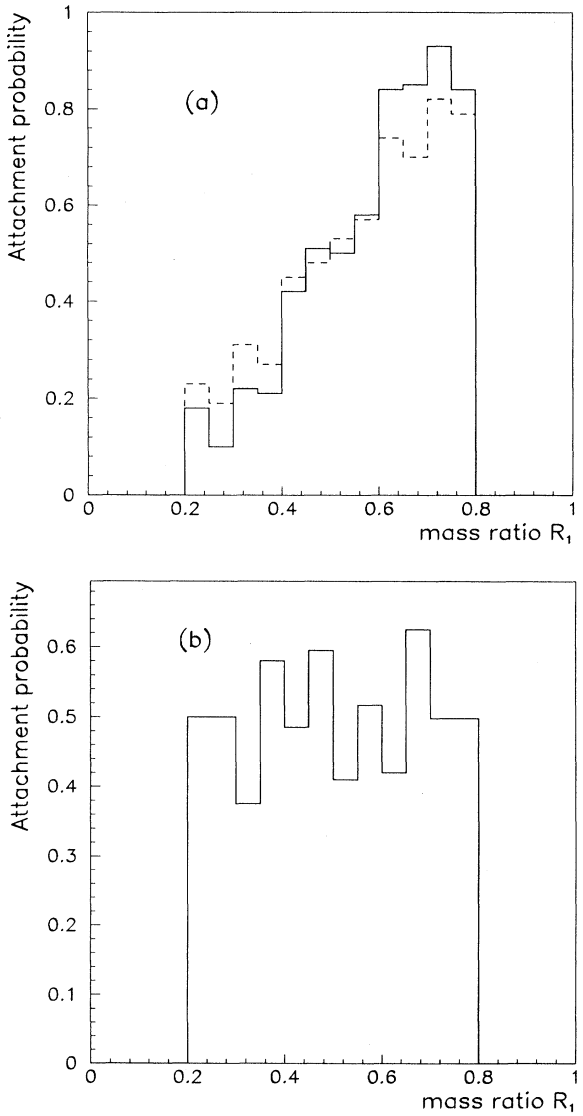

FIG. 8. Counting ratio $N_{F\Lambda}(R_1)/[N_{F\Lambda}(R_1) + N_{F\Lambda}(R_2)]$ vs the ratio $R_1 = M_1/(M_1 + M_2)$ for the shadow events (dashed line). The solid line represents this ratio after efficiency correction for (a) events with a high-amplitude MCP signal, and (b) events with a low-amplitude MCP signal.

Λ-hyperon sticking to fragments. The mass distribution of fission fragments quoted in the previous section was used. We neglect details of the interaction of the two nucleons produced in the nonmesonic decay, and assume that the distribution of the momentum transfer k to the fragment is described by the function

$$N(k) = k/\{1 + \exp[(k - k_0)/\Delta k]\} , \quad (4)$$

where k_0 and Δk are free parameters. The low momentum part of the distribution corresponds to those cases when both nucleons either transfer all their energy to the residual nucleus or are emitted without interacting with the residual nucleus. The high momentum part of the distribution includes those events when the high momentum tail of the nucleon momentum distribution is involved or when the energy released in the nonmesonic decay is carried away by an alpha particle or a heavier fragment.

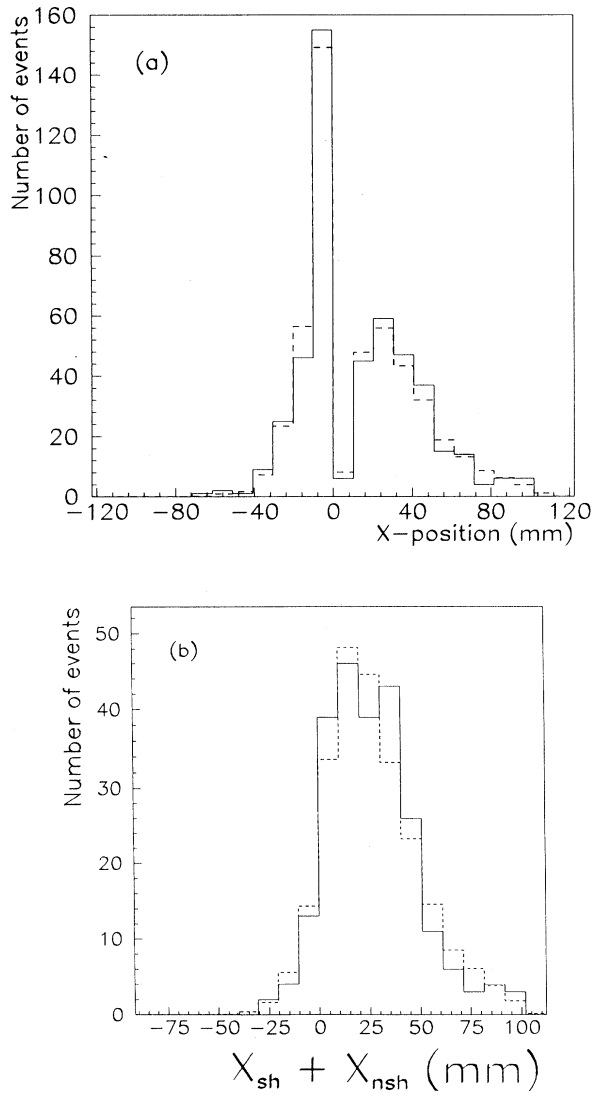

FIG. 9. Distributions for the fragments from prompt hypernucleus fission, (a) X position in the PPAC's, and (b) $(X_{sh} + X_{nsh})$. The solid line corresponds to the experimental data and the dashed line is the result of the simulation.

In Figs. 9(a) and 9(b) the solid lines show the experimental distribution of the X coordinate of both fragments and of the quantity $(X_{sh} + X_{nsh})$, respectively, where X_{sh} and X_{nsh} are the X coordinates in the shadowed and nonshadowed areas of the PPAC's. The latter distribution is related to the projection of the recoil momentum on the X axis. The dashed histograms in Figs. 9(a) and 9(b) are best fits from the Monte Carlo calculations corresponding to $k_0 = 350$ MeV/c and to $\Delta k = 150$ MeV/c. The p_0 was found to be equal to 450 MeV/c. The cutoff values for the momentum transfer in the $\bar{p}$ annihilation and in the nonmesonic hyperon decay were 2000 and 1000 MeV/c, respectively. Lower cutoff values do not give a good description of the experimental data. It was also checked that these results show a very weak dependence on the lifetime of hypernuclei of fission fragments.

C. Delayed fission

The aim of the analysis of the data on delayed fission was to estimate the lifetime of hypernuclei undergoing nonmesonic Λ-hyperon decay. Here we used the fact that only the position distribution in the X coordinate, perpendicular to the target plane, is sensitive to the lifetime. The analysis of this distribution for delayed fission was carried out assuming that it is entirely determined by the lifetime of hypernuclei and their momentum distribution. Consequently, in the Monte Carlo simulation we generated only the projection of the momentum perpendicular to the target plane. In so doing we employ a phenomenological approach, ignoring all details related to the production and scattering of hypernuclei in the target.

The Monte Carlo simulation of the delayed fission of heavy hypernuclei showed that in a broad range of lifetimes the X distribution in the shadow region remains steep at any distance from the target plane. The flat part of the experimental distribution in the shadowed area (see Fig. 6) may include the above-discussed background events due to the prompt fission of impurities on the MCP-detector holder (see Sec. II). This background could be excluded in the analysis on the basis of the arguments discussed in the following.

In the case of delayed fission of hypernuclei, coincidences of fragments are only recorded when the projection of the nuclear recoil on the X axis is positive, i.e., the momentum is directed downstream of the target. On the other hand, fragments resulting from the prompt fission of impurities on the MCP are detected (in coincidence) only if the momentum transferred to the fissioning nucleus is directed upstream of the target. As a result the quantity $(X_{sh} + X_{nsh})$ should be negative for the background while it is mainly positive for good events. It can be negative, sometimes, due to the kinematics of the Λ decay. However, the fraction of these events, as follows from a Monte Carlo simulation is small.

In Fig. 10(a) we show the measured X distribution of the shadow events with low-amplitude signals from the MCP detector (solid line) constructed with the condition $(X_{\rm sh} + X_{\rm nsh}) > 0$ imposed. We can see that after imposing this cut the distribution becomes steeper than the initial one (Fig. 6). In Fig. 10(b) we show the measured $(X_{\rm sh} + X_{\rm nsh})$ distribution.

In our Monte Carlo calculation we assumed that the momentum distribution of the recoils has the form given in Eq. (1). The cutoff parameter, $p_{\rm max}$, was 1200 MeV/c. The analysis has shown that for lower values of this cutoff, we cannot satisfactorily describe the experimental position distribution.

The parameter values which correspond to the best description of the experimental X distribution are $\tau = (1.25 \pm 0.15) \times 10^{-10}$ sec and $p_0 = (350 \pm 50)$ MeV/c. This value of the lifetime ($\chi^2 = 15.7$ for 13 degrees of freedom) was found to be very little dependent on the value of p_0.

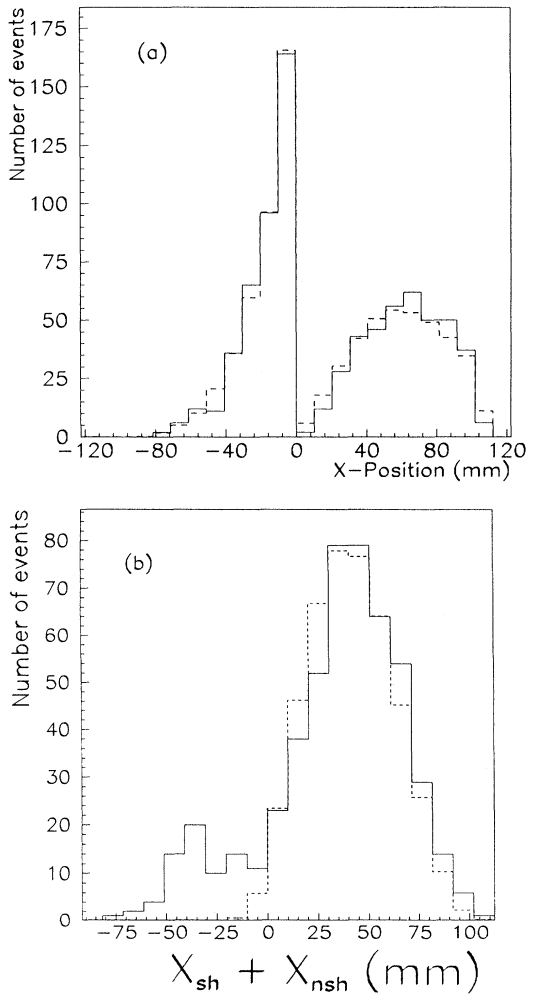

FIG. 10. Distributions for the fragments from delayed hypernuclear fission, (a) X position in the PPAC's of the fragments with $(X_{\rm sh} + X_{\rm nsh}) > 0$, and (b) $(X_{\rm sh} + X_{\rm nsh})$. The solid line corresponds to the experimental data and the dashed line is the result of the simulation.

In Fig. 10(a) the dashed line shows the X distribution calculated with the imposed condition $(X_{\rm sh} + X_{\rm nsh}) > 0$. The distribution $(X_{\rm sh} + X_{\rm nsh})$ calculated with these parameters reproduces well the data with $(X_{\rm sh} + X_{\rm nsh}) > 0$ [Fig. 10(b)].

To check the result on the hypernucleus lifetime, another procedure of calculation was used. This procedure was applied both to the present data for uranium and to the previously registered data for bismuth [2]. The range of a heavy nucleus can be written as

$$\mathbf{r} = \mathbf{V}_{\rm recoil} \times \tau \ , \tag{5}$$

where $\mathbf{V}_{\rm recoil}$ is the recoil velocity, and τ the lifetime. This does not require any knowledge of the recoil momentum distribution and gives the mean value of the lifetime if one knows the mean recoil velocity and the mean range. The recoil velocity and the lifetime are uncorrelated. Projecting on the beam axis X one obtains, for the mean lifetime,

$$\langle \tau \rangle = \frac{\langle r_X \rangle}{\langle (\mathbf{V}_{\rm recoil})_X \rangle} \ . \tag{6}$$

The experimental position distribution in the shadowed region is well reproduced if the range distribution r_X is taken as an exponential.

The mean recoil velocity is given by

$$\langle \mathbf{V}_{\rm recoil} \rangle = \frac{1}{2} \langle \mathbf{V}_1^{\rm lab} + \mathbf{V}_2^{\rm lab} \rangle \ , \tag{7}$$

where $\mathbf{V}_1^{\rm lab}$ and $\mathbf{V}_2^{\rm lab}$ are the velocities of the two fission fragments in the laboratory system. The projection of the recoil velocity on the beam axis X is

$$\langle (\mathbf{V}_{\rm recoil})_X \rangle = \frac{1}{2} \langle |\mathbf{V}_1^{\rm lab}| \cos\theta_1 + |\mathbf{V}_2^{\rm lab}| \cos\theta_2 \rangle \ , \tag{8}$$

where $\theta_{1,2}$ are the angles between the fragment trajecto-

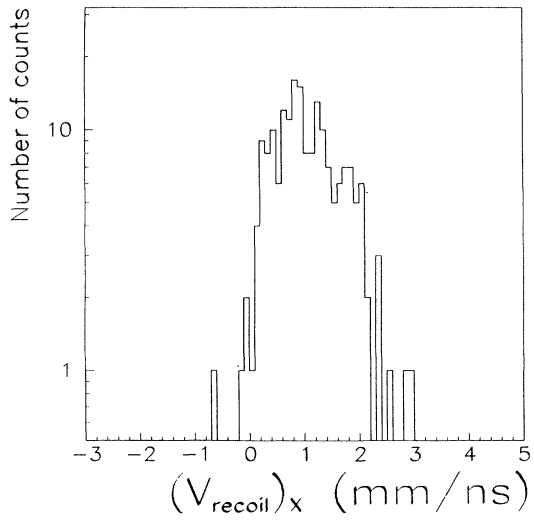

FIG. 11. Distribution of the X component of the recoil velocity as deduced from the measured fragment velocities.

TABLE I. Results obtained using the "mean" method both for the U (present data) and Bi (1986 data) targets. The systematical errors are given within parentheses.

Target	$\langle X \rangle$ (mm)	$\langle (V_{\text{recoil}})_X \rangle$ (mm/ns)	$\langle \tau \rangle$ (nsec)
Bismuth	$0.14\ ^{+0.020}_{-0.025}$	0.79± 0.05 (± 0.25)	0.18± 0.04 (± 0.06)
Uranium	$0.125\ ^{+0.019}_{-0.015}$	0.95± 0.07 (± 0.23)	0.13± 0.03 (± 0.03)

ries and the beam axis. The measured velocity spectra of fission fragments were calibrated by using the mean velocity of fragments in the laboratory system, 1.2 ± 0.1 cm/nsec [9]. Figure 11 shows the calculated distribution of the recoil velocity projection. Table I summarizes the mean values of the range, recoil velocity, and corresponding lifetimes for hypernuclei in the regions of Bi and U.

We can see that the lifetime for U quoted in Table I agrees well with that obtained in the Monte Carlo simulation. The lifetimes of Bi and U hypernuclei are smaller than the free Λ lifetime. In Fig. 12 we display the results for Bi and U together with the lifetimes of the free Λ hyperon and of $^{11}_{\Lambda}$B and $^{12}_{\Lambda}$C [10].

The position distribution of the shadow events detected with the target on a wide backing was measured without separating heavy hypernuclei from hypernuclei of fission fragments. The reason was that the MCP detector did not function well in this final stage of the experiment. The number of events of each type was estimated with a Monte Carlo calculation using the parameters obtained with the data from the narrow backing target. Their sum agrees within the statistical error with the number of events measured. This confirms our interpretation of the observed effects.

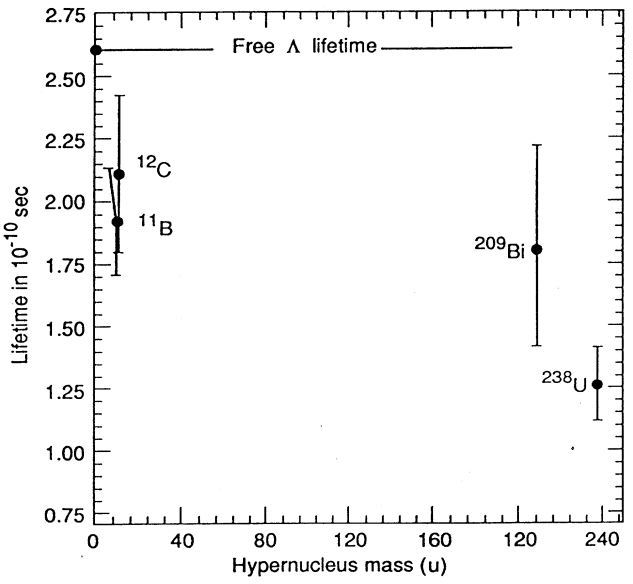

FIG. 12. Lifetime of hypernuclei as a function of their mass. (^{12}C and ^{11}B data are from Ref. [10], ^{209}Bi and ^{238}U are from this work.) Only statistical errors are given.

D. Yields

In order to estimate the yield of the processes studied here, it is necessary to know the efficiencies of detection for each process, and the number of antiprotons stopped in the target. The latter can be deduced from the fraction of the beam impinging on the target and from the stopping power of the target material.

The detection efficiency of single fragments from prompt fission was obtained in a Monte Carlo simulation which took into account the solid angle of the PPAC's. and the measured decrease of the counting rate for the fragments emitted at a small angle with respect to the target plane. This decrease is due to absorption and multiple scattering of the fragments in the target. The detection efficiency, including solid angle, is 0.05 for each PPAC. It decreases to $(3.4 \pm 0.4) \times 10^{-3}$ when the fragments are measured in coincidences.

The detection efficiency of hypernuclei of fission fragments is determined by the same factors as that for prompt fission but is strongly reduced (20 times). This is due to the fact that only a small fraction of the fragments are deviated to the shadowed area of the PPAC's, as a result of Λ decay. It was found to be $(1.7 \pm 0.2) \times 10^{-4}$.

The detection efficiency of delayed-fission fragments is essentially determined by the recoil-distance distribution of hypernuclei and was obtained from a Monte Carlo simulation equal to $(4.2 \pm 0.4) \times 10^{-3}$. It has to be corrected for the absorption of recoil nuclei in the target. This effect was estimated from a comparison of the yields of hypernuclei for two targets, 100 and 200 μg/cm^2 thick. We found that about 50% of the recoils are stopped in the 200 μg/cm^2 thick target. Consequently the detection efficiency of heavy hypernuclei produced in this target was $(2.1 \pm 0.7) \times 10^{-3}$.

Table II gives the number of registered events N_{expt}, the detection efficiencies ε, the corresponding number of events produced in the target, N_{target}, and the calculated yields Y per stopped antiproton of the three processes: prompt fission (PF) and the delayed and prompt fission of hypernuclei (DHF) and (PHF). The accuracy of the calculation of the yields of prompt and delayed hypernucleus fission is mainly determined by the error in the evaluation of the number of antiprotons passing through the target ($\sim$ 15%). In the case of heavy hypernuclei the main uncertainty ($\sim$ 30%) comes from the estimate of the number of recoil hypernuclei absorbed in the target.

TABLE II. The yields of prompt fission and hypernucleus formation in $\bar{p}$ annihilation on ^{238}U.

	PF	PHF	DHF	PHF+DHF
N_{expt}	625 358	238	438	676
ε	$(3.4 \pm 0.4) \times 10^{-3}$	$(1.7 \pm 0.2) \times 10^{-4}$	$(2.1 \pm 0.7) \times 10^{-3}$	$\times$
N_{target}	$(1.84 \pm 0.22) \times 10^{8}$	$(14 \pm 2) \times 10^{5}$	$(21 \pm 7) \times 10^{4}$	$(16 \pm 3) \times 10^{5}$
Y	0.85±0.15	$(6.5 \pm 1.3) \times 10^{-3}$	$(9.6 \pm 3.4) \times 10^{-4}$	$(7.4 \pm 1.7) \times 10^{-3}$

V. DISCUSSION

In the discussion of the results obtained, we first present those facts which support the hypernucleus-production hypothesis. They are the following: (i) the deviation of the prompt-fission fragment from its initial trajectory towards the shadowed zone of the PPAC's, (ii) the predominant detection of heavy prompt-fission fragments in the shadowed area, and (iii) the symmetric mass distribution for delayed-fission fragments.

As was shown in Sec. IV B, to explain the position and $(X_{\text{sh}} + X_{\text{nsh}})$ distributions for the prompt-fission fragments which hit the shadowed zone of the PPAC's, it is necessary to assume that a momentum up to a few hundred MeV/c is transferred to the fragment in flight. Such an effect can occur if a Λ hyperon decays with a lifetime of about 10^{-10} sec and, as a result of this decay, neutrons or protons are emitted with momenta close to 400 MeV/c. The only other particles which can be emitted from a fission fragment with such a lifetime are photons but the momentum transfer in this case is too small (1–2 MeV/c) to explain the experimental observation.

The fact that predominantly heavy prompt-fission fragments are registered in the shadowed zone of the PPAC's agrees with the hypothesis that the excited hypernuclei sometimes undergo fission. The depth of the potential well for the Λ hyperon is independent of the mass of the nucleus [11]. Therefore it is reasonable to expect that in the course of separation of the two fragments the Λ particle would stick to the fragment with larger volume, i.e., to the heavy fragment. However, no dependence on the fragment mass is expected in the case of delayed fission induced by the decay of the Λ particle from the recoiling hypernucleus. These expectations are consistent with the experimental results [see Figs. 8(a) and 8(b)].

The delayed fission observed cannot be explained on the basis of nuclear-structure effects, and, in particular, by the decay of fission isomers. The main argument completely excluding any isomeric state is that the delayed fission observed is characterized by the symmetric-fission mode. In order to induce symmetric fission of nuclei in the vicinity of uranium the excitation energy of the fissioning nucleus should be equal to several tens of MeV. No metastable states of nuclei exist with such excitation energy, and fission isomers are located in the 2–3 MeV region [12]. Thus, the decay of a Λ particle in a nucleus is the only plausible explanation to the delayed fission observed. To these arguments in favor of the hypernuclear hypothesis, we can add the fact that we earlier observed delayed fission in the annihilation of antiprotons in Bi [2]; no fission isomers exist in this region of nuclei.

While the events recorded by the PPAC's can be explained without any particular assumption on the Λ production mechanism from the $\bar{p}$ annihilation in uranium, the data obtained with the kaon detector should be analyzed only after assuming some specific mechanism for this production. Supposing that the hypernucleus is produced in the secondary interaction of kaons with nucleons of the residual nucleus, the number of expected coincidences between the selected shadow events and K^+ can be written

$$N_{K^+} = N_{\text{sh}} f \varepsilon \ , \tag{9}$$

where N_{sh} is the number of selected shadow events, f is the fraction of K^+ in the K mesons produced in association with the Λ particles, and ε is the kaon detection efficiency.

The efficiency for identifying K^+ with the KRT in the momentum range 250–750 MeV/c was determined from the inclusive number of K^+ per annihilation measured in experiment PS183 [13] with a uranium target, and from the number of K^+ detected in coincidence with the prompt-fission events. It was found to be $(1.1 \pm 0.2)\%$. With an estimated branching ratio of $f = K^+/(K^+ + K^0) = 0.43$ for annihilation on the uranium nucleus, we predict $N_{K^+} = 5$. It is unlikely that the error on this number is purely statistical, as its prediction is model dependent and hence subject to systematic error.

For example, in making this prediction, no angular correlations were assumed. The recoil-distance method is more efficient for those nuclei with momenta directed perpendicular to the target plane. Therefore, we can expect from momentum conservation that kaons in coincidence with fission events are emitted preferentially in a direction perpendicular to the target plane. Since the KRT was located at 90° to the target plane, the expected number of kaon-delayed fission coincidences may be reduced by about a factor of 2. Zero events were observed.

As was indicated in the previous section, it is possible to obtain a good description of the experimental data on the delayed fission with a cutoff of the momentum transfer in the $\bar{p}$ annihilation at 1200 MeV/c. This value is in good agreement with the upper limit of the recoil momentum distribution calculated by Cugnon *et al.* [14]. Therefore, we assume that the observed heavy hypernuclei are predominantly hypernuclei of uranium isotopes

with masses slightly below 238, as found in Ref. [14]. On the other hand, in the case of hypernuclei of fission fragments, the required minimum cutoff value for the recoil momentum is 2000 MeV/c (see Sec. IV B). This value is consistent with the fact that about 18 neutrons are emitted in the $\bar{p}$-induced fission [7]. As a result the required cutoff for the momentum transfer in the case of heavy hypernuclei becomes higher.

From Table II we can see that the total hypernucleus-formation probability per stopped antiproton is about 7.4×10^{-3}. The yield of hypernuclei in the $\bar{p}$ annihilation in uranium was estimated in Ref. [14] to be 9.7×10^{-3}, which is consistent with our present result. It can be compared with the measured Λ^0 production rate in complex nuclei given in Ref. [15] to be $(1.9 \pm 0.4)\%$ per stopped antiproton. From this, one may deduce that in $\bar{p}$ annihilation on heavy nuclei (i) the Λ^0 production rate accounting for hypernuclear formation is $(2.6 \pm 0.5)\%$, and (ii) the probability of the Λ attachment to a heavy nucleus is about 25%. This is very close to the value found in reactions with stopped K^- ($\sim 30\%$, Ref. [16]).

VI. CONCLUSION

The main results of the present experiment are the following. (i) The annihilation of antiprotons in ^{238}U leads to the production of hypernuclei of fission fragments and of heavy hypernuclei in the region of uranium. (ii) The lifetime of the heavy hypernuclei is found to be $(1.25 \pm 0.15) \times 10^{-10}$ sec. (iii) When the fission of an excited hypernucleus occurs, the Λ hyperon predominantly sticks to the heavy fragment; this fact can be used in the analysis of the dynamics of fission [17]. (iv) The probability of Λ-hyperon attachment to a heavy nucleus, following $\bar{p}$ annihilation, is estimated to be about 25%. (v) We do not find with significant confidence that K^+ are produced in coincidence with the hypernuclear events. However, this conclusion depends on complex and poorly known features of kaon production in heavy nuclei.

ACKNOWLEDGMENTS

This experiment has benefitted from the high quality technical support from CERN. We express our gratitude in particular to N. Mezin and J. Place who carried out the mechanics and to the LEAR group for their continuous effort on beam settings. We are also indebted to B. Gay for his help in high vacuum matters. We thank N. Trautmann (Mainz University) who prepared the Cf source, H. Folger (GSI), and D. Ledu (CSNSM-Orsay) who prepared the targets. We acknowledge fruitful discussions with J. Cugnon and J. Vandermeulen. The Swedish participants (G. E., T. J., and G. T.) are indebted to the Swedish Natural Science Research Council for support. The U.S. part of this work was supported by the Air Force Office of Scientific Research under Grant No. 87-0246.

APPENDIX

The count rate $N_{F\Lambda}(R_1)$ of fission fragments observed in the shadowed region, in coincidence with a complementary fragment in the open region, a high-amplitude MCP signal, and a corresponding mass ratio R_1 can be written

$$N_{F\Lambda}(R_1) = N_{\rm HN} P_{\rm pf} F(R_1) A_\Lambda(R_1) \eta_{\rm MCP} \epsilon(R_1) \ ,$$

where $N_{\rm HN}$ is the production rate of hypernuclei; $P_{\rm pf}$ is the probability that a hypernucleus undergoes prompt fission, the lambda remaining attached to one of the fragments; $F(R_1)$ is the probability that the fragments of mass m_1 and m_2 are produced [obviously $F(R_1) = F(R_2)$]; $A_\Lambda(R_1)$ is the attachment probability of the lambda particle to fragment of mass m_1; $\eta_{\rm MCP}$ is the detection efficiency, very close to unity, of the secondary electron detector when two fission fragments emerge from the target; and $\epsilon(R_1)$ is the probability that one of the fission fragments is detected, after deflection due to the lambda decay, in the shadowed area and the other fragment in the open area of the parallel plate detector.

By definition $A_\Lambda(R_1) + A_\Lambda(R_2) = 1$. It follows that

$$\mathcal{A}_{\rm expt}(R_1) = \frac{N_{F\Lambda}(R_1)}{N_{F\Lambda}(R_1) + N_{F\Lambda}(R_2)} = \frac{A_\Lambda(R_1)\epsilon(R_1)}{A_\Lambda(R_1)\epsilon(R_1) + A_\Lambda(R_2)\epsilon(R_2)}$$

and

$$\mathcal{A}_{\rm cor}(R_1) = \frac{\frac{N_{F\Lambda}(R_1)}{\epsilon(R_1)}}{\frac{N_{F\Lambda}(R_1)}{\epsilon(R_1)} + \frac{N_{F\Lambda}(R_2)}{\epsilon(R_2)}} = A_\Lambda(R_1) \ ,$$

where $\mathcal{A}_{\rm expt}$ and $\mathcal{A}_{\rm cor}$ are the experimental and efficiency corrected ratios.

[1] J.P. Bocquet, M. Epherre-Rey-Campagnolle, G. Ericsson, T. Johansson, J. Konijn, T. Krogulski, M. Maurel, E. Monnand, J. Mougey, H. Nifenecker, P. Perrin, S. Polikanov, C. Ristori, and G. Tibell, Phys. Lett. B **182**, 146 (1986).

[2] J.P. Bocquet, M. Epherre-Rey-Campagnolle, G. Ericsson, T. Johansson, J. Konijn, T. Krogulski, M. Maurel, E. Monnand, J. Mougey, H. Nifenecker, P. Perrin, S. Polikanov, C. Ristori, and G. Tibell, Phys. Lett. B **192**, 312 (1987).

[3] J. Cugnon and J. Vandermeulen, Phys. Lett. **146B**, 16 (1984); Ann. Phys. (Paris) **14**, 49 (1989).

[4] V. Metag, E. Liukkonen, G. Sletten, O. Glomset, and S. Bjørnholm, Nucl. Instrum. Methods **114**, 445 (1974).

[5] H.G. Clerc, H.J. Gehrhardt, L. Richter, and K.H. Schmidt, Nucl. Instrum. Methods **113**, 325 (1973).

[6] T.A. Armstrong, D.M. Elias, R.A. Lewis, E.D. Minor, J. Passaneau, and G.A. Smith, Nucl. Instrum. Methods A

289, 109 (1990).
[7] J.P. Bocquet, F. Malek, H. Nifenecker, M. Rey-Campagnolle, M. Maurel, E. Monnand, P. Perrin, C. Ristori, G. Ericsson, T. Johansson, G. Tibell, S. Polikanov, T. Krogulski, and J. Mougey, Z. Phys. A **342**, 183 (1992); B. Chen, T. A. Armstrong, R. A. Lewis, R. Newton, G. A. Smith, J. P. Bocquet, F. Malek, H. Nifenecker, M. Maurel, E. Monnand, P. Perrin, C. Ristori, G. Ericsson, T. Johansson, G. Tibell, M. Rey-Campagnolle, S. Polikanov, T. Krogulski, and J. Mougey, Phys. Rev. C **45**, 2332 (1992).
[8] F. Malek, Thèse Université Joseph Fourier, Grenoble, France, 1990.
[9] V.E. Viola, Jr., Nucl. Data **A1**, 391 (1966).
[10] R. Grace, P.D. Barnes, R.A. Eisenstein, G.B. Franklin, C. Maher, R. Reider, J. Seydoux, S. Bart, R.E. Chrien, P. Pile, Y. Xu, R. Hackenburg, E. Hungerford, B. Bassalleck, M. Barlett, E.C. Milner, and R.L. Stearns, Phys. Rev. Lett. **55**, 1055 (1985).
[11] B. Povh, Annu. Rev. Nucl. Part. Sci. **28**, 1 (1978).
[12] S. Bjørnholm and J.E. Lynn, Rev. Mod. Phys. **7**, 52 (1980); **7**, 25 (1980).
[13] E.D. Minor, T.A. Armstrong, R. Bishop, V. Harris, R.A. Lewis, and G.A. Smith, Z. Phys. A **336**, 461 (1990).
[14] J. Cugnon, P. Deneye, and J. Vandermeulen, Phys. Rev. C **41**, 1701 (1990).
[15] G.T. Condo, T. Handler, and H.O. Cohn, Phys. Rev. C **29**, 1531 (1984).
[16] M. Csejthey-Barth, G. Schorochoff, and P. Van Binst, Nucl. Phys. **B14**, 330 (1969).
[17] H. Nifenecker and F. Malek, Nucl. Phys. **A531**, 539 (1991).